Antioxidant and Anticancer Activities and Protein Interaction of the Oxidovanadium(IV) Naringin Complex

Andrés Gonzalo Restrepo-Guerrero [1], **Helen Goitia-Semenco** [1], **Luciana G. Naso** [1], **Marilin Rey** [2], **Pablo J. Gonzalez** [2], **Evelina G. Ferrer** [1] **and Patricia A. M. Williams** [1,*]

1 Centro de Química Inorgánica (CEQUINOR, UNLP, CONICET, Asociado a CICPBA), Departamento de Química, Facultad de Ciencias Exactas, Universidad Nacional de La Plata, Bv. 120 N° 1465, La Plata B1906, Argentina; gonzalo.restrepo@quimica.unlp.edu.ar (A.G.R.-G.); helengoitia@quimica.unlp.edu.ar (H.G.-S.); luciananaso504@hotmail.com (L.G.N.); evelina@quimica.unlp.edu.ar (E.G.F.)

2 Departamento de Física, Facultad de Bioquímica y Ciencias Biológicas, Universidad Nacional del Litoral and CONICET, Santa Fe S3000, Argentina; mrey@fbcb.unl.edu.ar (M.R.); pablogonzalez1979@gmail.com (P.J.G.)

* Correspondence: williams@quimica.unlp.edu.ar

Abstract: The complex of oxidovanadium(IV) with naringin (Narg) [VO(Narg)$_2$] 8H$_2$O (VONarg) was prepared according to the literature improving the synthetic procedure and physicochemical characterization. In addition, biological activities (cytotoxic, antioxidant, and BSA interaction) were determined. The metal coordinated through the 5-hydroxy and 4-carbonyl groups of rings A and C of naringin, respectively. The antioxidant activity of VONarg, determined in vitro, was higher than those of the flavonoid against superoxide and peroxyl reactive oxygen species (ROS) and DPPH radical. The cytotoxic properties were determined by a MTT assay on adenocarcinoma human alveolar basal epithelial cells (A549). VONarg exerted a 20% decrease in cancer cells viability at 24 h incubation, while naringin and oxidovanadium(IV) cation did not show cytotoxicity. Measurements with the normal HEK293 cell line showed that the inhibitory action of the complex is selective. VONarg generated intracellular reactive oxygen species (ROS), depletion of reduced glutathione and depolarization of mitochondrial membrane potential, typical for apoptotic pathway, producing cell death by oxidative stress mechanism. Moreover, naringin interacted with bovine serum albumin (BSA) through hydrophobic interactions in a spontaneous process, and VONarg showed greater affinity for the protein but can still be transported and delivered by it (K$_a$ 10^4 L·mol^{-1} order).

Keywords: glycosylated flavonoid; oxidovanadium(IV) complex; antitumoral; antioxidant

1. Introduction

Flavonoids are an important group of natural substances, containing phenolic structures, which can be found in fruits, vegetables, and some beverages [1]. They are benzo-γ-pyrone derivatives consisting of aromatic (A and B) and pyrene (C) rings (Figure 1A) and are classified according to structural changes in hydroxylation pattern, conjugation between the aromatic rings, glycosidic moieties, and methoxy group [2,3]. These secondary metabolites have shown many and different applications, such as antiviral activity against zika virus infection [4], anti-hyperglycemic, liver protective [5], and anti-rheumatoid arthritis effects [6], antigenotoxic activity [7], and modulation of cardiovascular K$^+$ channels [8], just to mention some cutting-edge studies from the last few years. It is also well known these compounds have anti-oxidative, anti-inflammatory, anti-mutagenic, and anti-carcinogenic properties coupled with their capacity to modulate the cellular key and enzyme function [1].

Another important feature of flavonoids is their capacity to chelate metal ions and form coordination complexes through hydroxyl and keto groups [9]. There are three main chelating sites for metal ions in flavonoids, e.g., the 3′,4′-dihydroxy group located on the B ring, the 3-hydroxy or 5-hydroxy, and the 4-carbonyl group in the C ring [3]. In

glycosylated flavonoids, metal coordination can also take place through hydroxy groups of the saccharide moiety [10].
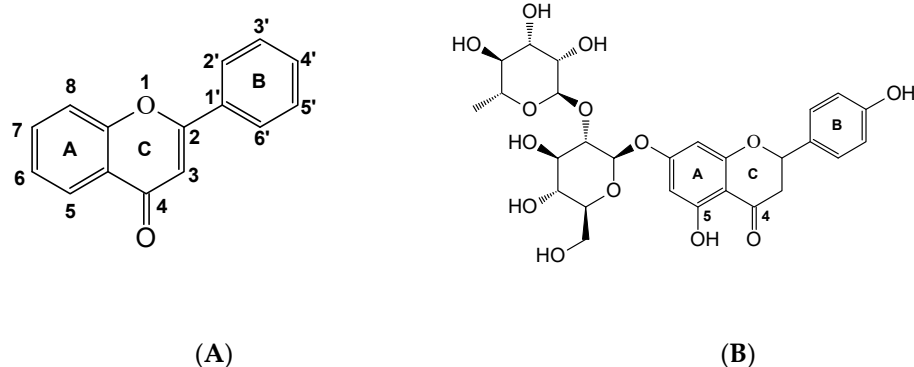

Figure 1. (**A**) Flavone structure. (**B**) Naringin structure.

Naringin (Figure 1B) is a natural flavanone glycoside biosynthesized via the phenyl-propanoid pathway from shikimic acid [11]. It is mainly found in citrus fruits, such as grapefruits, lemons and oranges [12], also apples, onions, and tea [13]. Recent studies have demonstrated its numerous in vivo and in vitro properties exerting potential therapeutic effects by modulating various protein and enzyme expressions [14]. It possesses properties such as anti-inflammatory effects [15,16], oxidative stress reduction [17,18], and it has proven to be one potential anticancer agent against different types of cancer and also acted synergistically enhancing the anticancer activities of antitumor drugs in combination therapies [19]. Molecular docking studies showed that naringin interacted with COVID-19 main protease and displayed higher binding affinity than other flavonoids [20].

Metal-flavonoid chelates have a considerably better biological activity than their flavonoid and metal precursors on their own and we have reported this behavior in previous works with other flavonoids, such as hesperidin, diosmin, and rutin and their oxidovanadium(IV) complexes [21–23].

Vanadium derivatives have shown insulin-mimetic, antidiabetic properties, and anti-tumor properties; vanadium compounds are promising non-platinum anticancer agents due to their low IC_{50}, low toxicity, along with antiproliferative, genotoxic, and proapoptotic effects by modulation of important protein function and reactive oxygen species (ROS) action [24].

Naringin is capable of binding the oxidovanadium(IV) cation through two different sites (the flavonoid or the saccharide moiety). At the experimental conditions selected herein, we have modified the structure of the ligand at the flavonoid moiety (pH 9) and compared the physicochemical, antioxidant, cytotoxic, and protein interaction properties of both the complex and the ligand.

2. Results

2.1. Characterization of V(IV)O–Naringin Complex

2.1.1. Fourier Transformed Infrared Spectroscopy

The FTIR main vibrational bands of naringin and the oxidovanadium(IV) complex are presented in Table 1. The assignments were performed according to general references of VOflavonoid systems [21]. Similar broad bands for the ligand and the complex and assigned to the OH stretching modes (including OH groups of crystallization H_2O for the complex) could be seen at the 3400–3200 cm^{-1} region. The band due to C=O stretching at 1645 cm^{-1} shifted in the complex to 1637 cm^{-1} because of the coordination of this group to the metal ion that produced a decrease in bond order and an increase in bond length. The bands related to the C=C stretching modes of the aromatic group (1630–1500 cm^{-1}) showed the expected changes due to the resonance established by coordination with the oxidovanadium(IV) cation. Modes involving OH stretching and COH bending (1360–1000 cm^{-1})

were modified and/or reduced the intensities due to deprotonation or coordination of the C_5-OH group, indicating the interaction of the metal center through this group: the bending COH modes at 1355 cm^{-1} and 1341 cm^{-1} appeared at 1357 cm^{-1}, the band at 1295 cm^{-1} decreased its intensity and the bands at 1281 cm^{-1} and 1265 cm^{-1} shifted to 1256 cm^{-1}. Bands related to C-O stretching also decreased their intensities. However, the band related to C-O stretching of the sugar moiety at 1074 cm^{-1} did not change upon metal coordination to naringin, indicating that the glycoside group did not participate in the coordination. Moreover, the V=O stretching appeared at 980 cm^{-1} as with naringenin (VONar), so the typical coordination through 5-O$^-$ and 4-C=O groups of A and C rings of naringin, respectively, can be assumed and the coordination of the metal center through the sugar moiety can be discarded. In this latter case, the V=O stretching appeared at low energies (ca. 920 cm^{-1}) [25]. This band appeared overlapped with the band of the ligand at 987 cm^{-1}, previously assigned to V=O stretching.

Table 1. Assignment of the FTIR spectra of naringin and the oxidovanadium(IV) complex (band positions in cm^{-1}) [a].

Naringin	VONarg	Vibrational Modes-Functional Groups
3422 br 3231 sh	3395 br 3205 sh	ν O-H
1645 vs	1637 sh	ν C=O ring C
1629 sh 1615 sh	1614 vs	ν C=C
1582 m	1574 vs 1537 m	ν C=C
1520 m 1504 m	1520 m	ν C=C
1355 sh 1341 m	1357 sh	δ COH
1295 m	1292 w	δ HOC
1281 w 1265 w	1256 w	δ HOC, ν (C-O-C)
1134 s	1134 m	ν C-O secondary alcohol
1074 vs	1076 vs	ν O-C sugar
1062 vs	1060 sh	ν C-O primary alcohol
1041 vs	1040 sh	ν O-C
987 m	987 m	ν O-C
	980 m	ν V=O
822 m	814 w	ν C-C, ν O-C

[a] vs, very strong; s, strong; m, medium; w, weak br, broad; sh, shoulder.

2.1.2. Powder and Frozen Solution EPR Spectra

The powder EPR spectrum of the VONarg complex obtained at 120 K is shown in Figure 2A. The spectrum consisted of a weak—although detectable—signal with a hyperfine structure produced by the I = 7/2 nuclear spin from magnetically isolated V^{4+} ions (inset of Figure 2A), superimposed with a broad resonance line attributed to metal sites with spin–spin exchange interactions between neighboring V^{4+} sites.
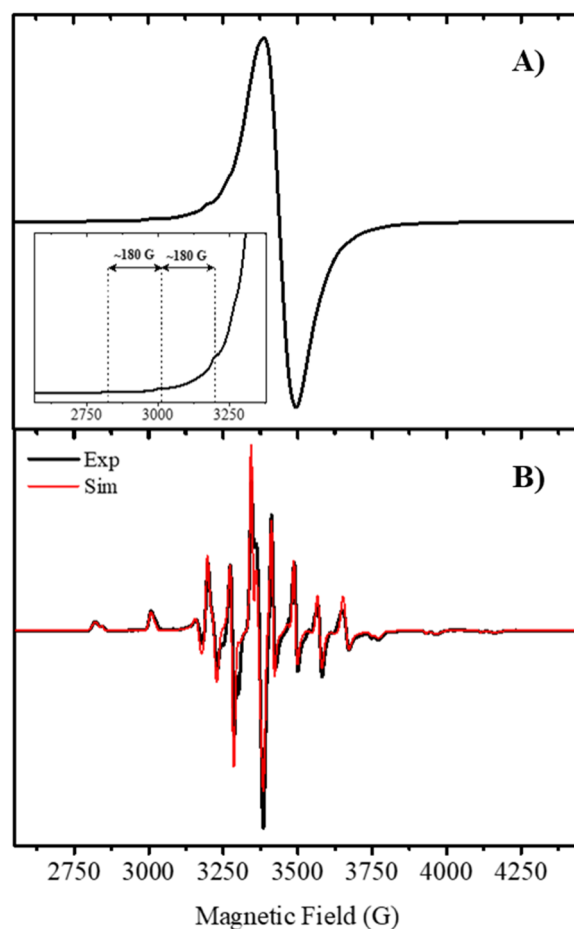
Figure 2. EPR spectrum of VONarg: (**A**) Powdered sample at 120 K, (**B**) Experimental spectrum (black) and simulation (red) of frozen pure DMSO solution at 120 K.

The EPR spectra of the frozen solutions in both pure DMSO and in H_2O/DMSO mixtures (ratios 50/50, 90/10, and 99/1, pH ca. 7) measured at 120 K showed minor differences than that obtained in pure DMSO (see Figures 2B and S1). They showed the typical axial spectrum with a hyperfine structure produced by the ^{51} V nucleus. The spectrum seemed to be composed of two species (labeled as S1 and S2) with different contributions (1:0.2). Simulations yielded the spin Hamiltonian parameters shown in Table 2.

Table 2. Spin Hamiltonian parameters obtained from simulations.

	$g_{\parallel}$	$g_{\perp}$	[1] $A_{\parallel}$	[1] $A_{\perp}$	$\Delta g_{\parallel}/\Delta g_{\perp}$	[1] P	k	[1] $P \times k$
S1	1.9332	1.9717	167.0	62.8	2.26	121.8	0.72	87.3
S2	1.9398	1.9751	159.4	51.6	2.30	125.8	0.62	78.2

[1] A, P and $P \times k$ are given in $\times 10^{-4}$ cm^{-1}.

For both S1 and S2 the $g_{\parallel} < g_{\perp} < g_e = 2.0023$ and $|A_{\parallel}| > |A_{\perp}|$, indicating an octahedral geometry with tetragonal compression with a d_{xy} ground state, and the ratio $\Delta g_{\parallel}/\Delta g_{\perp}$ indicated considerable tetragonal distortion. According to the empirical relationship $A_z = \sum(n_i \cdot A_{z,i})$ used to determine the identity of the equatorial ligands in V(IV) complexes (accuracy of $\pm 3 \times 10^{-4}$ cm^{-1}) (n_i, number of equatorial ligands of type i and $A_{z,i}$, the contribution to the parallel hyperfine coupling from each of them) [26], and considering the contributions to the parallel hyperfine coupling constant of the different coordination modes (CO = 44.7×10^{-4} cm^{-1}, ArO$^-$ = 38.6×10^{-4} cm^{-1}), S1 was consistent with the pro-

posed structure, with 2 C=O and 2 ArO$^-$ moieties in the equatorial plane ($A_\parallel$ = 166.6 cm^{-1}) that should correspond to a square pyramidal geometry. However, a decrease in A_{II} (as in Table 2) was found by Gorelsky et al. [27] when the solvent coordinated to V=O in the axial position, so it could be proposed that DMSO (or the solvent H_2O) may coordinate to the sixth position, *trans*- to the metal center, in S2. However, vanadium coordination to the sugar moieties with (O$^-$O$^-$) donor set (A_{II} ca. 155–157 × 10^{-4} cm^{-1}), could not be ruled out [22,28].

Using the relations developed by Kivelson and Lee [29],

$$A_\parallel = -P\left[k + \frac{4}{7} - \Delta g_\parallel - \frac{3}{7}\Delta g_\perp\right] \tag{1}$$

$$A_\perp = -P\left[k - \frac{2}{7} - \frac{11}{4}\Delta g_\perp\right] \tag{2}$$

the *p*-value (dipolar hyperfine coupling parameter) that represents the dipole–dipole interaction of the electronic and nuclear moments can be obtained. *p*-values range from 100 to 160 × 10^{-4} cm^{-1} in oxidovanadium(IV) compounds [30] and are calculated as $P = g_e g_N \mu_B \mu_N \langle r^{-3}\rangle$, where g_N is the nuclear g-factor, g_e is the g-factor of the free electron, μ_N the nuclear magneton, and $\langle r^{-3}\rangle$ can be calculated for the vanadium 3d orbitals. The parameter k is the dimensionless Fermi contact interaction constant, ranging from 0.6 to 0.9 [31], is very sensitive to deformations of the metal orbitals, and indicates the isotropic Fermi contact contribution to the hyperfine coupling. The calculated values of p = 120–125 × 10^{-4} cm^{-1} (Table 2) were considerably reduced when compared to the value of the free ion (160 × 10^{-4} cm^{-1}) and indicated a considerable amount of covalent bonding in the complex. The values of k = 0.62–0.72 indicated a moderate contribution to the hyperfine constant by the unpaired s-electron.

2.1.3. Spectrophotometric Titrations

The spectral bands for the visible part of the spectrum of the complex in DMSO, located at 598 nm and 810 nm are typical for VOflavonoid complexes interacting by the 4-carbonyl and 5-hydroxy groups of rings A and C (Figure 1) [32]. Spectrophotometric titration in DMSO was performed at different ligand-to-metal ratios from 0.5 to 10.0 and pH 9. The absorbance of the band at 810 nm in the electronic spectra was monitored at each molar ratio. From Figure 3, a L:M 2:1 stoichiometry was determined.
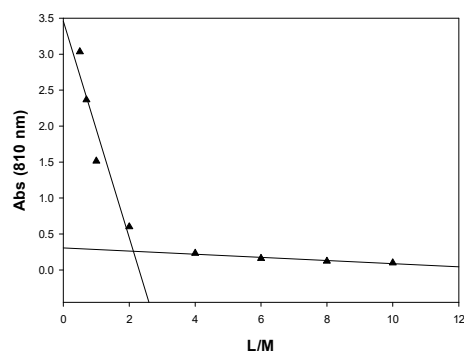

Figure 3. Spectrophotometric titration of V^{IV}O^{2+} with naringin at pH = 9, under nitrogen atmosphere. L/M, naringin/ V^{IV}O^{2+} molar ratio. Absorbance at 810 nm.

2.2. Antiradical Behavior

For biological studies, it is important to measure, in the first instance, the stability of the complex. The stability of VONarg in DMSO solution was followed by UV-vis spectroscopy and conductivity measurements over time. Both the spectral pattern (Figure S2A) and the molar conductivities (data not shown) did not change at least during the first 15 min of manipulation (for biological studies), demonstrating that the compounds were stable

in DMSO. Although a spectral shift due to solvatochromic effects was observed between DMSO and DMSO/water (1/99) solutions, the complex behaved in the same way as DMSO during the first 15 min (Figure S2B).

From Table 3 an enhancement on the superoxide dismutase (SOD) activity of the complex concerning naringin can be observed, but the effect was still low (IC$_{50}$ = 870 μM), hence, the complex could not be considered as a good SOD simil agent. The scavenging activity for peroxyl radical (ROO$^{\bullet}$) was enhanced by complexation. The complex caused a delay in pyranine consumption (lag phase) by the ROO$^{\bullet}$ radical of 3.8 min at 100 μM. However, this delay was not so effective as that produced by the reference compound Trolox. No antiradical effect against hydroxyl (OH$^{\bullet}$) was measured for the complex, though naringin produced a 30% scavenge of hydroxyl radical at 100 μM concentration. Oxidovanadium(IV) complexation showed much stronger 2,2′-diphenyl-1-picrylhydrazyl radical (DPPH$^{\bullet}$) scavenging than the ligand, and the same effect has previously been reported for the copper/naringin metal complex [33]. In summary, metal complexation improved the antioxidant behavior of the flavonoid against the ROS superoxide and peroxyl and also against the DPPH$^{\bullet}$ radical. These results were obtained when the coordination, as in VONarg, occurred through C=O and deprotonated O moieties (from 4-carbonyl and 5-hydroxyl, respectively). This acetylacetonate-type coordination enhanced π delocalization between V=O and the ligand, which conferred a high capacity to stabilize unpaired electrons and then scavenge free radicals. However, the antioxidant behavior of naringin was moderate because of the lack of a double bond between C2 and C3 and the absence of this double bond also forbids the electronic resonance of the generated radicals with ring B and only ring A was involved in π delocalization with the metal center.

Table 3. Percentage of free radical scavenging of naringin, VONarg, and oxidovanadium(IV) cation. Values are expressed as the mean ± standard error of at least three independent experiments.

Radical	% Scavenging		
	Naringin	**VONarg**	**V(IV)O^{2+}**
SOD (IC$_{50}$, μM)	>1000	870 ± 5.2	15 ± 0.2
ROO$^{\bullet}$, lag (min), 100 μM	0	3.8 ± 0.8	6.4 ± 1.1
OH$^{\bullet}$, 100 μM	28 ± 0.4	0	38 ± 2
DPPH$^{\bullet}$, 100 μM	2.0 ± 0.7	45.0 ± 5.0	37.0 ± 2

IC$_{50}$ SOD$_{native}$ = 0.21 μM; lag phase Trolox, 37.28 min.

2.3. Anticancer Effects

Numerous studies have shown that naringin inhibits cell proliferation and induces apoptosis in a majority of tumor cells, including breast cancer (TNBC), human cervical cancer (SiHa), and 5637 bladder cancer cells [19]. The cytotoxicity of the compounds was investigated by the MTT assay. Results are expressed as a percent with respect to control values. In particular, in the human lung cancer A549 cells naringin induced no cytotoxicity at the tested concentrations (up to 500 μM at 24 h incubation). On the contrary, VONarg reduced cell viability in a dose response manner with a 20% reduction at 100 μM (Figure 4) and 40% at 500 μM. In addition, the oxidovanadium(IV) cation did not show significant cytotoxic effects up to 100 μM, 24 h incubation [34]. Moreover, the complex did not reduce the cell viability of the non-tumorigenic HEK293 cell line (0–100 μM) (Figure S3).

In addition, alterations in cell morphology as a consequence of the exposition to VONarg were observed using Giemsa staining (Figure 5). Control A549 cells displayed a typical epithelial-like morphology. Upon treatment with VONarg, 100 μM concentration for 24 and 48 h, different degrees of morphological changes were observed. The complex caused cytoplasmic shrinkage, elongated lamellipodia, and moderate cell population decrease at 24 h incubation. The formation of apoptotic bodies was observed at 48 h

incubation. It can be seen that the cytotoxic effect of the complex was greatly increased with the incubation time.
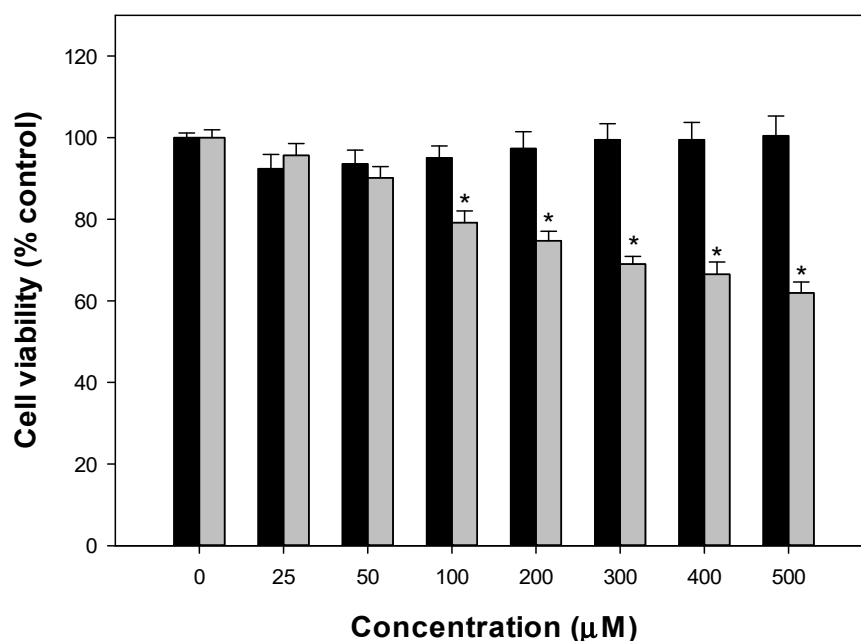

Figure 4. Effects of naringin (black) and VONarg (grey) on A549 cell line viability. Cells were incubated in serum-free Dulbecco's modified Eagle's medium (DMEM) alone (control) or with different concentrations of the compounds at 37 °C for 24 h. The results are expressed as the percentage of the control level and represent the mean ± SEM. * Significant difference with control at the 0.05 level.
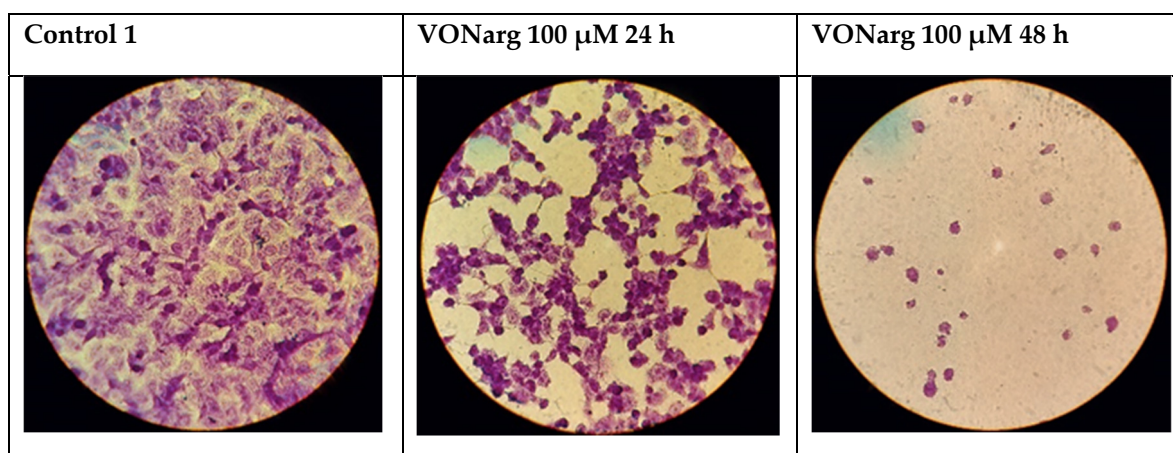

Figure 5. Effect on cell morphology for the treatment of A549 cell line with VONarg. Cells were incubated for 24 and 48 h without drug additions (control) and with the complex (100 μM, 400× *g* magnification).

It is known that cell growth and death are regulated by the redox status of the environment and excessive production of ROS and low GSH levels induce apoptosis or necrosis. To evaluate if the toxic mechanism of action occurs through the induction of intracellular ROS production, A549 cells incubated with different doses of the compounds were assessed using the oxidant-sensitive dye H_2DCFDA. From Figure 6, it can be seen that while naringin did not generate excessive cellular ROS levels, VONarg produced an increase in ROS (250% of the control level at 100 μM and 24 h incubation). Furthermore, the oxidovanadium(IV) cation did not produce ROS in the A549 cell line, 24 h incubation [34].
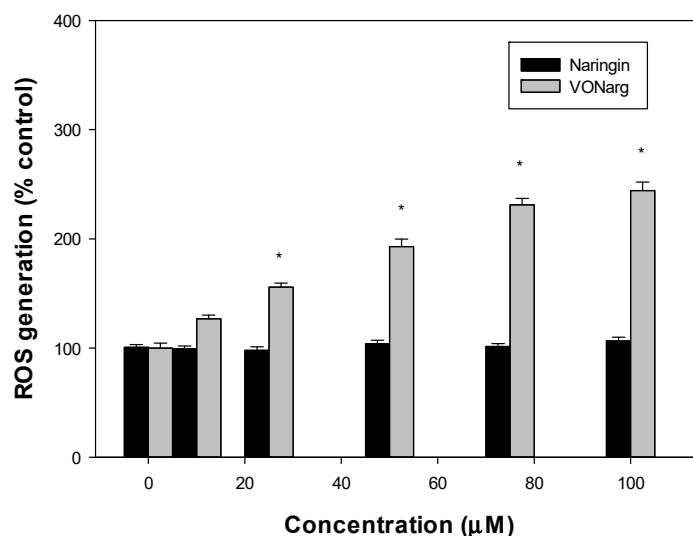
Figure 6. Effects of naringin (black) and VONarg (grey) on H_2DCFDA oxidation to DCF. A549 cells were incubated at 37 °C in the presence of 10 μM H_2DCFDA. The values are expressed as the percentage of the control level and represent the mean ± SEM. * significant difference with control at the 0.05 level.

GSH is one of the natural antioxidants that prevent the oxidation of cellular components. Cellular redox imbalance is also demonstrated by the reduction in endogenous GSH production at the same time that cells are producing increased levels of ROS. When the tripeptide non-protein thiol compound, GSH, acted as a defense system against oxidative stress it oxidized to GSSG. Therefore, GSH/GSSG ratio is a better signal of oxidative stress generation. Treatment with VONarg caused a decrease in GSH and the GSH/GSSG ratio levels in a dose–response manner (Figure 7).
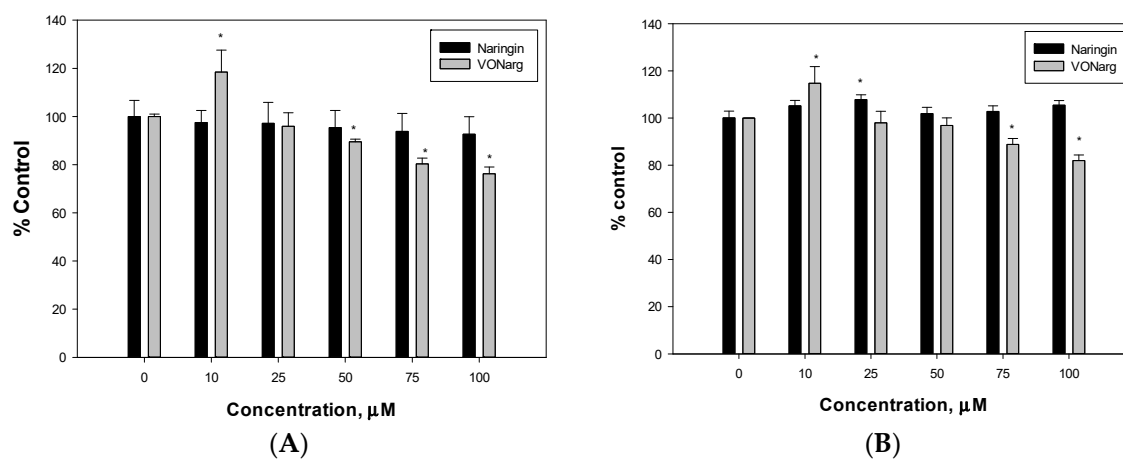

Figure 7. Effect of naringin and VONarg on GSH cellular levels (**A**) and GSH/GSSG ratio (**B**) in A549 cells. Results are expressed as mean ± SEM of three independent experiments, * significant differences in comparison with the control level ($p < 0.05$).

To elucidate the mechanism of action of the complex under oxidative stress conditions, the mitochondrial membrane potential at different concentrations of VONarg was measured (Figure 8). $DioC_6$ is a lipophilic cationic probe that is able to enter into the mitochondria and when depolarization occurs, it will accumulate less dye. VONarg caused mitochondrial depolarization as evidenced by the decrease in membrane potential in response to the damage produced by ROS increment. Then, VONarg could induce apoptosis of A549 cells by activating mitochondrial death pathways related to ROS and GSSG generation.
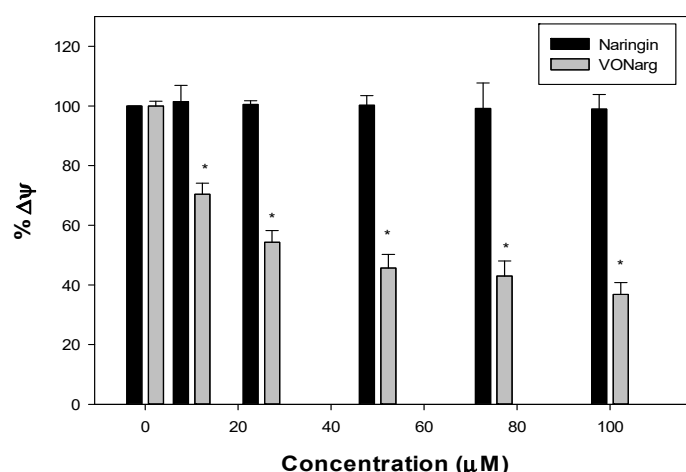
Figure 8. Changes of the mitochondrial membrane potential (% Δψ) in A549 cells treated with increasing concentrations naringin (black) and VONarg (grey) for 24 h. Each point represents the mean ± S.E.M of three measurements in three independent experiments. Significant differences: * *p* < 0.05 compared to the control.

2.4. Bovine Serum Albumin (BSA) Interactions

Many drugs circulate reversibly in the bloodstream bound to plasma protein. Human serum albumin is the best carrier for acidic and neutral drugs and influences their pharmacokinetics and pharmacodynamics. It can be used in cosmetics, food technology, crop protection, industrial chemical processes, having great potential in pharmacology because of its ability to increase solubility for lipophilic drugs, allowing their interaction with the site of action. Thus, the interaction of a drug with plasma proteins is a relevant factor influencing the distribution, elimination, duration, and intensity of their pharmacological activities [35]. Consequently, the albumin-binding assay may provide some information for the pathway for bioactive compound transportation. In this sense, bovine serum albumin (BSA) is often used as a model to study in vitro interactions because of its similarity to HSA, stability, low cost, and intrinsic fluorescence properties originated by two tryptophan residues (Trp-134 and Trp-212). BSA is very sensitive to the alteration of its tertiary structure, and this effect can be followed by fluorescence spectroscopy.

To analyze the binding affinity of naringin and VONarg the fluorescence spectra of BSA were recorded in the presence of increasing quantities of the flavonoid and the complex in the 5–100 μM range. As shown in Figure 9, the increment of the concentration of naringin and VONarg at 298 K produced a quenching process on the intrinsic albumin fluorescence. The reduction in fluorescence intensity suggests BSA-compound interactions and that, at the same concentration value, the effect of the quenching process is higher for the VONarg complex than the flavonoid. The observed intensity of fluorescence (F_{obs}) was corrected because the UV absorbance of the samples can decrease the observed values (inner-filter effect) [36,37]. Considering the absorbances at the exciting and emitted radiation A_{ex} and A_{em}, respectively, the corrected fluorescence intensity (F_{corr}) was determined using the following equation: $F_{corr} = F_{obs} \times e^{(A_{ex} + A_{em})/2}$.

Fluorescence quenching can be static or dynamic. In the static one, there exists a complex formation between the quencher and the fluorophore, while a collision process is described for the dynamic one. The Stern–Volmer equation was applied to determine the type of fluorescence quenching:

$$F_0/F = 1 + K_q \tau_0[Q] = 1 + K_{sv}[Q] \tag{3}$$

where F_0 and F are the fluorescence intensities in the absence and presence of the quencher, respectively; K_q is the bimolecular quenching constant; τ_0 is the lifetime of the fluorophore in the absence of the quencher (usually taken as 1×10^{-8} s); [Q] is the concentration of the

quencher and K_{sv} is the Stern–Volmer quenching constant. The calculated curves of F_0/F vs. [Q], depicted in Figure S4, showed a linear dependence that suggests a single quenching process, either static or dynamic. The K_{sv} values presented in Table 4 showed a slight increase correlated with temperatures and the calculated quenching rate constants (K_q) were higher than the limiting diffusion rate constant (2.0×10^{10} L·mol^{-1}·s^{-1}). Thus, the most probable quenching mechanism was initiated by the ground-state complex formation (static quenching), but the possible existence of combined quenching cannot be ruled out [38].
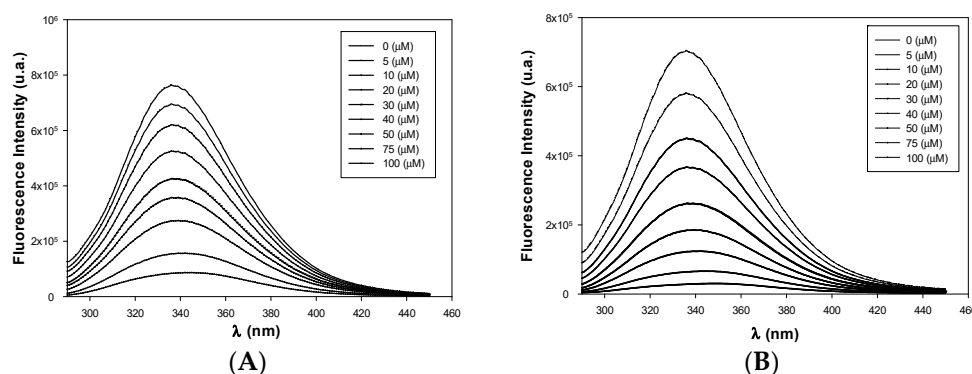

Figure 9. Fluorescence spectra of BSA in the presence of (**A**) naringin and (**B**) VONarg in Tris–HCl buffer of pH 7.4 at 298 K. BSA (6 μM), naringin and VONarg (0–1.00 μM).

For a fluorescence quenching of protein with a static quenching process, the free and bound molecule equilibrium can be analyzed by the following equation:

$$\log[(F_0 - F)/F] = \log K_b + n \log [Q] \tag{4}$$

where K_b is the binding constant (displaying the interaction degree of BSA and the quencher) and n is the number of binding sites (Table 4).

Figure 10 shows the resulting $\log [(F_o - F)/F]$ vs. $\log [Q]$ plots. The same tendency of the K_b constant with temperature increments can be seen and higher K_b values of VONarg in comparison with naringin support the strong interaction with the albumin for the complex at the same temperature. In addition, reversible binding to BSA is inferred based on the obtained values lying in the 10^4 to 10^6 M^{-1} range and it is possible that VONarg remained stable in the biological systems and could be carried by albumin [39]. The n value (approximately equal to 1) suggests the existence of one independent class of binding sites on BSA for both compounds. Moreover, it has been determined that naringin interacted with BSA at the named Sudlow's site I within the hydrophobic pocket of subdomain IIA, mainly through hydrophobic interactions [40].

Table 5 shows the K_b binding values for naringin, its aglycon naringenin and their oxidovanadium(IV) and palladium(II) complexes. It is known that glycosylation of flavonoids lowered the binding affinity for BSA. The change in the planar structure due to the replacement of the hydroxyl group by the disaccharide neohesperidose may cause steric hindrance diminishing affinity for BSA [42]. Indeed, according to the obtained K_b values, the affinity of naringenin for BSA was about 7-fold higher than naringin. The complexes showed a different behavior. The reported Pd complex and VONarg, both containing naringin displayed greater K_b values than the oxidovanadium(IV) complex of naringenin. Therefore, the presence of naringin favors the interaction with albumin in these complexes.
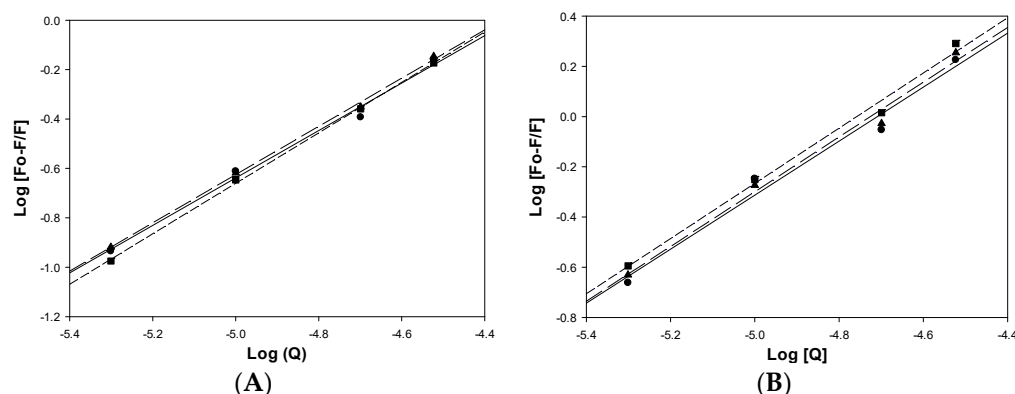
Figure 10. Plots of log $(F_o - F)/F$ vs. log [Q] for the naringin-BSA system (**A**) and VONarg-BSA system (**B**): (●) 298 K; (▲) 303 K; (■) 310 K, [BSA] = 6 μM, λ_{ex} = 280 nm.

Table 4. Stern–Volmer constant (K_{sv}), quenching rate constant (K_q), binding constant (K_b), and n binding sites for the interaction of naringin and VONarg with BSA (6 μM) in Tris–HCl buffer (pH 7.4).

	T (K)	K_{sv} (10^4) (L·mol^{-1})	K_q (10^{12}) (L·mol^{-1}s^{-1})	K_b (10^4) (L·mol^{-1})	n
Naringin *	298	2.18 ± 0.15	2.18 ± 0.15	1.45 ± 0.23	0.96 ± 0.03
	303	2.28 ± 0.09	2.28 ± 0.09	1.81 ± 0.44	0.98 ± 0.10
	310	2.32 ± 0.13	2.32 ± 0.13	2.81 ± 0.38	1.02 ± 0.09
VONarg	298	5.67 ± 0.33	5.67 ± 0.33	11.6 ± 0.19	1.08 ± 0.04
	303	5.88 ± 0.31	5.88 ± 0.31	14.1 ± 0.13	1.09 ± 0.03
	310	5.99 ± 0.36	5.99 ± 0.36	16.9 ± 0.19	1.10 ± 0.04

r^2 (correlation coefficient) values are all ranged from 0.977 to 0.999 for the K_{sv}, K_q, and K_b constants. * K_{sv} and K_b values are in the same order of magnitude as those from literature [40,41].

Table 5. K_b binding values for naringenin, naringin, VO(naringenin)$_2$·H$_2$O, VONarg and [Pd{(C,N)-C$_6$H$_4$CH$_2$NH(Et)(Narg)]} complexes at 298 K.

Compounds	$K_b \times 10^4$ M^{-1}
Naringenin *	10.20
naringin	1.45
VO(naringenin)$_2$·H$_2$O *	0.31
VONarg	11.6
[Pd{(C,N)-C$_6$H$_4$CH$_2$NH(Et)(Narg)}] *	18

* Data taken from references [25,43].

The thermodynamics of the process for the formation of a complex between BSA and flavonoid and/or its metal complex can be determined from the dependence of the binding constant with temperature. Some non-covalent interactions may contribute to these interactions: hydrogen bonds, Van der Waals force, electrostatic and hydrophobic interactions. The changes in the thermodynamic parameters for the systems, free energy ΔG, enthalpy ΔH, and entropy ΔS, were analyzed to estimate the types of complex–protein binding at different temperatures. The enthalpy and entropy values were resolved from the relationship between ln K_b and $1/T$. The $\Delta H/R$ values were obtained from the slope, and from the intersection with the y axis, the $\Delta S/R$ values. Values of ΔG were then found as $\Delta G = -RT \ln K_b$.

The spontaneity of the processes was determined by the value of ΔG, while the combinations of the signs associated with ΔH and ΔS suggest the bonding strength. If

ΔH and ΔS values are negative they give evidence to the existence of hydrogen bonds and/or van der Waals forces. Electrostatic interactions are suggested for negative ΔH and positive ΔS values and hydrophobic interactions occur when both parameters display a positive sign.

The average values of the thermodynamic parameters are depicted in Table 6 where positive ΔH and ΔS values were found. Thus, the sign of ΔG implies spontaneity, and the ΔS value is the major contribution (entropically driven) in an endothermic process. However, the comparison of the values for both compounds suggests that the complex shifted to an environment of reduced hydrophobicity (-56% in ΔH value and -79% in a ΔS value).

Table 6. Thermodynamic parameters for the systems naringin-BSA and VONarg-BSA.

Compounds	ΔH (KJ/mol)	ΔS (J/mol)	ΔG (KJ/mol)
Naringin	42.7	222.7	−23.7 (298 K) −24.8 (303 K) −26.3 (310 K)
VONarg	23.9	177.0	−28.8 (298 K) −29.7 (303 K) −31.0 (310 K)

3. Discussion

We have synthesized the oxidovanadium(IV) complex of naringin using different techniques, as previously reported [44] and extended the physicochemical characterization. The vibrational spectral characterization of the naringin complex with the oxidovanadium(IV) cation showed an acetylacetonate coordination mode (C_4=O, C_5-O$^-$). EPR determinations in solution (DMSO and H_2O/DMSO mixtures) support this coordination mode with square pyramidal geometry (90%), and most likely, a distorted octahedral with DMSO in *trans*-position (10%). It was shown by electronic spectroscopy that the complex was stable in DMSO and DMSO/water (1/99), at least during the manipulation time. The stability of the complex in DMSO was also shown by molar conductivity determinations.

Natural polyphenols showed antioxidant properties that were enhanced by metal complexation (see Section 2.2) because of the increased stability of the free radical generated in the first step of their oxidation by electron delocalization with the V=O orbitals. This behavior was also displayed by VONarg. Previously, we have studied the biological improvement of naringenin (aglycone of naringin) by oxidovanadium(IV) complexation (VONar) [25]. Antioxidant determinations showed that VONar is somehow a better antioxidant compound (only the peroxyl radical scavenging activity is low, lag phase VONar = 2.9 min, a 100 µM). Glycosylation on C7-OH may disrupt the electron delocalization of the free radical generated when that H atom is abstracted in the aglycone form.

Cancer cells, with a pro-oxidant status, seem to be more susceptible to treatment with agents that cause oxidative stress than normal cells. Excessive ROS production, exceeding a threshold level, can lead to cellular damage and induce cell death and it has been shown that many compounds exert anticancer activity by cellular ROS generation [45]. Accordingly, in the present study, we studied cellular ROS production and GSH/GSSG depletion in the human lung A549 cancer cell line, showing that the ROS generation by the complex was accompanied by the oxidation of the natural antioxidant agent GSH to give GSSG, being this behavior different from what occurred in the in vitro determinations (Section 2.2). It has to be noted that naringin at 100 µM did not show cytotoxic activity towards A549 cancer cells, in agreement with reported results [46,47] nor did it produce or deplete cellular ROS, and it did not generate oxidized glutathione. On the other hand, the oxidovanadium(IV) cation did not generate ROS in the A549 cell line (100 µM, 24 h incubation) [35] nor deplete GSH, showing that the anticancer effect is only due to the effect of metal complexation of the flavonoid. A similar enhancement of the decrease in cell viability upon complexation was shown for naringin-Ag(I) and -Y(III) in A549 cell line, 48 h incubation [48].

Because one of the major events during apoptosis is the depolarization of the mitochondrial membrane, which subsequently induces the release of the proapoptotic proteins [49], we measured if the complex could damage the mitochondrial membrane. Treatment of A549 cells with VONarg induced a significant loss of $\Delta\Psi$m and may cause A549 cell apoptosis. Then, it has been demonstrated that the complex can be toxic to cancer cells inducing ROS production and GSH depletion and the loss of $\Delta\Psi$m. On the other hand, the complex of naringenin, VONar, significantly decreased the viability of lung cancer cells in a dose–response manner (35% at 100 μM) but in both cases, the IC_{50} values were higher than 100 μM [25]. Flavonoids with C2-C3 double bond exert better anticancer effects [50]. The low anticancer activities of both compounds could be supported by the structure of the flavonoid: the lack of the C2-C3 double bond forbids the electronic delocalization between rings B and C. However, we found an improvement in the cytotoxic effects of both flavonoids upon metal complexation, due to the planar structure produced by the resonance of ring B with the V=O moiety. The interaction with BSA was spontaneous, entropically driven, and the obtained value of the binding constant suggests that albumin could act as a carrier for the transport in plasma and delivery to target cells of VONarg.

4. Material and Methods

4.1. Materials and Instrumentation

Naringin (Sigma, St. Louis, MO, USA), oxidovanadium(IV) chloride (50% aqueous solution, Carlo Erba, Buenos Aires, Argentina), bis(acetylacetonato)oxidovanadium(IV) (Fluka, Munich, Germany), and oxidovanadium(IV) sulfate pentahydrate (Merck) were used as supplied. Corning or Falcon provided cell culture materials. Dulbecco's modified Eagle's medium (DMEM) was purchased from Gibco (Gaithersburg, MD, USA), Tryple^{TM} from Invitrogen (Buenos Aires, Argentina SRL), and fetal bovine serum (FBS) from Internegocios, Buenos Aires, Argentina. All other chemicals used were of analytical grade. Elemental analysis for carbon and hydrogen was performed using a Carlo Erba EA1108 analyzer. Vanadium content was determined by the tungstophosphovanadic method [51]. Thermogravimetric analysis (TGA) was performed with a Shimadzu thermobalance (model TG-50), working in an oxygen flow of 50 mL/min, and at a heating rate of 10 °C/min. Sample quantities ranged from 10 to 20 mg. UV-vis and diffuse reflectance (BaSO$_4$ as standard) spectra determinations were recorded with a Shimadzu UV-2600/2700 spectrophotometer. Infrared spectra were measured using the KBr pellet technique with a Bruker IFS 66 FTIR spectrophotometer from 4000 to 400 cm^{-1}. Fluorescence spectra were obtained with a Shimadzu RF-6000 spectrophotometer equipped with a pulsed xenon lamp. The molar conductance of the complex was measured using a Conductivity TDS Probe-850084, Sper Scientific Direct, using 10^{-3} M DMSO solutions. X-band CW-EPR spectra of both powdered samples and DMSO or DMSO/water solutions (pH ca. 7) were obtained at 120 K on a Bruker EMX-Plus spectrometer, equipped with a rectangular cavity with 100 kHz field modulation. EPR spectra were baseline corrected (when necessary) using the WinEPR Processing software (Bruker, Inc. Billerica, MA, USA). *g*- and *A*-values were obtained by simulations using the EasySpin 5.2.3 toolbox based on MATLAB [26], assuming an axial spin-Hamiltonian of the form: $H = \mu_B \left[g_\| B_z S_z + g_\perp \left(B_x S_x + B_y S_y \right) \right] + \left[A_\| S_z I_z + A_\perp \left(S_x I_x + S_y I_y \right) \right]$, where μ_B is the Bohr magneton, and $g_\|$, $g_\perp$, $A_\|$, $A_\perp$ are the components of the axial **g** and **A** tensors, respectively. $B_{x/y/z}$, $S_{x/y/z}$, and $I_{x/y/z}$ are the components of the magnetic field, and the spin operators of the electron and V nucleus, respectively.

4.2. Synthesis of [VO(Narg)$_2$]·8H$_2$O (VONarg)

The solid complex was prepared using different preparative methods than the reported one [44]. A solution of oxidovanadium(IV) sulfate pentahydrate in methanol (0.25 mmol, 5 mL) was dropwise added to a naringin methanolic solution (0.5 mmol, 20 mL). pH was then adjusted to 9 by the addition of 0.2 M NaOH drops in methanol. After 1 h of stirring (under nitrogen atmosphere), a yellow-greenish solid was precipitated by the addition of 100 mL of bidistilled water. The solid was filtered off and washed with plenty

of bidistilled water and dried at 60 °C. It was possible to obtain the same complex using a different synthetic method by adding 0.25 mmol of bis(acetylacetonato)oxidovanadium(IV) over a hot aqueous solution of naringin (80 °C). After 30 min of stirring (under nitrogen atmosphere), a yellow-greenish precipitate formed, it was filtered off, washed several times with hot bidistilled water, and dried at 60 °C. Due to the reduction in costs and waste production as well as its simplicity, the synthesis using hot water was employed to prepare the solid compound that was used to conduct all the other physiochemical characterizations. Anal calcd. For $C_{54}H_{78}O_{37}V$: C 47.33%; H 5.73%; V 3.71%; Found: C 47.1%; H 5.6%; V 3.9%; Yield: 51.62%. UV-Vis data for 1:2 VO:Naringin, DMSO: 598 nm ($3d_{xy} \rightarrow 3d_{x2-y2}$, $\varepsilon = 50.4$ M^{-1} cm^{-1}); 810 nm ($3dxy \rightarrow 3d_{xz}$, $3d_{yz}$, $\varepsilon = 60.3$ M^{-1} cm^{-1}). Thermal decomposition measurements gave the same results as reported by Badea et al. [44]. A first weight loss at 105 °C of 10.4% corresponded to the loss of 8 molecules of water ($\Delta\omega\%$ calc = 10.5%). The presence of V_2O_5 in the residue was confirmed by FTIR spectroscopy. The molar conductance of the complex measured in DMSO, $\Lambda m = 0$ ($\Omega^{-1}\cdot cm^2\cdot mol^{-1}$), suggested that it had a non-electrolytic nature. These results allowed us to postulate a L:M stoichiometry of 2:1 [52], which was also supported by spectral determinations (see below).

4.3. Spectrophotometric Titration

In order to establish VONarg stoichiometry, the molar ratio method was applied. A DMSO solution of naringin (2×10^{-2} M) was prepared and its electronic spectrum was recorded. The absorption spectra of different solutions of naringin (2×10^{-2} M) and oxidovanadium(IV) chloride in ligand-to-metal molar ratios from 10 to 0.5 (pH 9) were measured.

4.4. Antioxidant Properties

The antioxidant activities of the complex and the ligand were determined by the Superoxide Dismutase (SOD) mimetic assay, scavenging power of the hydroxyl radical, inhibitory action on peroxyl radical, and 1,1-Diphenyl-2-picrylhydrazyl radical (DPPH) assay. Reported protocols were used in these determinations [53]. Briefly, the nitrobluetetrazolium (NBT) assay was used to determine indirectly the SOD activity. The activity of naringin and VONarg for their ability to inhibit the reduction in NBT by the superoxide anion generated by the phenazinemethosulfate (PMS) and reduced nicotinamide adenine dinucleotide (NADH) system was measured. The 50% inhibition (IC_{50}) for naringin or VONarg was estimated by plotting the percentage of reduction in NBT versus the negative log of the concentration of the sample solution. The capacity of naringin and VONarg to scavenge hydroxyl radicals (generated by the ascorbate-Fe-H_2O_2 system) was measured by the determination of the extent of deoxyribose degradation by hydroxyl radical at 535 nm. The inhibitory activity against peroxyl radicals was determined by measuring the delay produced by the compounds on pyranine consumption (lag phase) from the peroxyl radicals. The DPPH radical scavenging activity was measured in the presence and absence of the compounds and this later value was assigned to 100%. Each experiment was performed in triplicate and at least three independent experiments were evaluated in each case.

4.5. Biological Assays

4.5.1. Cell Culture

Adenocarcinomic human alveolar basal epithelial cells (A549 cell line) were obtained from ABAC (Argentinean Cell Bank Association INEVH, Pergamino, Buenos Aires, Argentina). DMEM supplemented with 100 U·mL^{-1} penicillin, 100 µg·mL^{-1} streptomycin, and 10% (*v/v*) fetal bovine serum was used as culture medium. When 70–80% confluence was reached, cells were washed with phosphate-buffered saline (PBS) (11 mM KH_2PO_4, 26 mM Na_2HPO_4, 115 mM NaCl, pH 7.4) and were subcultured using TrypLE™. All reagents were from Sigma–Aldrich (St Louis, MO, USA). Cultures were maintained at 37 °C in a humidified atmosphere with 5% CO_2 and passaged, according to the manufacturer's instructions.

4.5.2. MTT Assay

Stock complex solutions of compounds were prepared in DMSO with a manipulation time of 15 min. A549 cells and HEK293 (human embryonic kidney) were seeded at a density of 15,000 cells/well in 96 well plates, grown overnight, and treated with either vehicle (DMSO), naringin, VONarg, or oxidovanadium(IV) in DMSO at different concentrations in DMEM supplemented with 100 U·mL^{-1} penicillin and 100 μg·mL^{-1} streptomycin. The dissolution vehicle yielded a maximum final concentration of 0.5% in the treated well. After 24 h of incubation, 3-(4,5-methyl-thiazol-2-yl)-2,5diphenyl tetrazolium bromide (MTT) (Sigma–Aldrich, St. Louis, MO, USA) was added at 100 μg/well for 2 h. The formazan products generated by cellular reduction of MTT were dissolved in DMSO and the optical density was measured at 450 nm using Sinergy 2 Multi Mode Microplater reader Biotek (Wisnooski, VT, USA). All experiments were done in triplicate. Data were presented as proportional viability (%) comparing the treated group with the untreated cells, for which the viability was assumed to be 100%.

4.5.3. Stress Oxidative Determinations

Generation of intracellular reactive oxygen species (ROS) was measured using a 2′,7′-dichlorodihydrofluorescein diacetate probe (H2DCF-DA, Sigma–Aldrich). The probe hydrolyzed by intracellular esterases to the non-fluorescent 2′,7′-dichlorodihydrofuorescein (H2DCF), and the cytosolic cellular oxidants oxidized H2DCF to the fluorescent product, dichlorofluorescin (DCF). Hence, DCF fluorescence intensity is proportional to the amount of ROS. Here, after 24 h incubation with the complex, the cells were incubated with 10 mM DCFH-DA (dissolved in PBS with 5% DMSO) at 37 °C for 60 min under light protection and then lysed with 1 mL Tryton X-100 0.1%. The intracellular ROS were detected at 485 nm for excitation and 520 nm for emission.

The effect of the complex on the intracellular glutathione (GSH) level was assessed using o-phthaldialdehyde (OPT) [54] that reacted with the amino and sulfhydryl groups of glutathione emitting intense fluorescence at pH 8 and 12. For the GSH assay, 100 mL aliquots of the treated cells were incubated with OPT (0.1% MeOH in cold phosphate buffer (Na$_2$HPO$_4$ 0.1 M, M-EDTA 0.005 M, pH 8)). For the oxidized glutathione (GSSG) determinations, 100 mL aliquots of the cellular lysate were incubated with 0.04 M *N*-ethylmaleimide (NEM) to block the thiol groups in GSH, followed by the addition of OPT solution and the incubation in NaOH 0.1 M solution. The fluorescence intensity was detected at 350 nm excitation and 420 nm emission. The data were normalized against the total protein content measured by the Bradford method [55]. The GSH and GSSG contents (Sigma–Aldrich) were calculated from a calibration curve from standard solutions.

The mitochondrial membrane potential analysis was assessed using the DiOC6 fluorescent probe (3,3′-dihexyloxacarbocyanine iodide), which was added to the wells (400 nM concentration) and incubated for 30 min at 37 °C. The cells were resuspended in PBS and measured at 485 nm excitation and 535 nm emission [56].

4.6. Data Analysis

All the experiments were performed in triplicate, and each one was repeated at least three times. All the values were expressed as the mean ± standard error. Differences between the mean values were analyzed for significance using the one-way ANOVA test on Origin 9.1 (OriginLab Corporation, Northampton, MA, USA). $p < 0.05$ values were considered to be statistically significant.

4.7. Bovine Serum Albumin Interactions

BSA was dissolved in Tris–HCl (pH 7.4) buffer to attain a final concentration of 6 μM, 10 mL. Naringin and VONarg, dissolved in 0.5% DMSO/buffer solution, were added dropwise to the BSA solution to obtain the desired concentration of 5 to 100 μM. The solutions were left into a thermostatic water bath for 1 h at 298, 303, and 310 K, to get homogeneous solutions and allow the interaction between compound and protein.

The compounds did not show any fluorescence intensity that could interfere with the measurements. BSA 6 μM was titrated by successive additions of naringin and VONarg solutions and the fluorescence intensity was measured on a luminescence spectrometer in the range from 290 to 450 nm. For each sample and concentration, three independent replicates were performed. All the fluorescence quenching data were analyzed according to previous studies performed in our laboratory applying the well-known Stern–Volmer equation and other traditional mathematical procedures were applied to obtain the Stern–Volmer quenching constant and the binding constant (K_b) and the binding site value (*n*) [25].

5. Conclusions

The V(IV)O-naringin complex was prepared and characterized in the solid state (EPR measurements) and solution (EPR spectrum, conductance, spectrophotometric titration, and stability studies). Metal coordination to positions 4 and 5 of the glycosylated flavonoid enhanced the moderate antioxidant activity of the ligand against superoxide and peroxyl ROS, which may be due to the higher electron delocalization induced by the resonance of the π bond of the oxidovanadium(IV) cation with ring A. In addition, the metal complex showed higher anticancer activity when compared to naringin through ROS elevation and GSH/GSSG decrease, enhancing the oxidative stress that led to mitochondrial damage and cell death. A selective anticancer behavior was found. BSA interaction studies showed a static quenching process and the binding constant values were indicative that the complex could be transported and delivered by the protein. The experimental results showed the potential of flavonoids' complexation with oxidovanadium(IV) cation to improve their biological actions.

References

1. Panche, A.N.; Diwan, A.D.; Chandra, S.R. Flavonoids: An overview. *J. Nutr. Sci.* **2016**, *5*, E47. [CrossRef] [PubMed]
2. Wang, T.Y.; Li, Q.; Bi, K.S. Bioactive flavonoids in medicinal plants: Structure, activity and biological fate. *Asian J. Pharm. Sci.* **2018**, *13*, 12–23. [CrossRef]
3. Dias, M.C.; Pinto, D.C.G.A.; Silva, A.M.S. Plant Flavonoids: Chemical Characteristics and Biological Activity. *Molecules* **2021**, *26*, 5377. [CrossRef]
4. Zou, M.; Liu, H.; Li, J.; Yao, X.; Chen, Y.; Ke, C.; Liu, S. Structure-activity relationship of flavonoid bifunctional inhibitors against zika virus infection. *Biochem. Pharmacol.* **2020**, *177*, 113962. [CrossRef]
5. Zhu, X.; Ouyang, W.; Lan, X.; Xiao, H.; Tang, L.; Liu, G.; Feng, K.; Zhang, L.; Song, M.; Cao, Y. Anti-hyperglycemic and liver protective effects of flavonoids from *Psidium guajava* L. (guava) leaf in diabetic mice. *Food Biosci.* **2020**, *135*, 100574. [CrossRef]
6. Sun, Y.W.; Bao, Y.; Yu, H.; Chen, Q.J.; Lu, F.; Zhai, S.; Zhang, C.F.; Li, F.; Wang, C.Z.; Yuan, C.S. Anti-rheumatoid arthritis effects of flavonoids from Daphne genkwa. *Int. Immunopharmacol.* **2020**, *83*, 106384. [CrossRef]
7. Tuentera, E.; Creylman, J.; Verheyen, G.; Pieters, L.; Van Miert, S. Development of a classification model for the antigenotoxic activity of flavonoids. *Bioorg. Chem.* **2020**, *98*, 103705. [CrossRef] [PubMed]
8. Fusia, F.; Trezza, A.; Tramaglino, M.; Sgaragli, G.; Saponara, S.; Spiga, O. The beneficial health effects of flavonoids on the cardiovascular system: Focus on K^+ channels. *Pharmacol. Res.* **2020**, *152*, 104625. [CrossRef]
9. Khater, M.; Ravishankar, D.; Greco, F.; Osborn, H.M.I. Metal complexes of flavonoids: Their synthesis, characterization and enhanced antioxidant and anticancer activities. *Future Med. Chem.* **2019**, *11*, 2845–2867. [CrossRef]
10. Allscher, T.; Klüfers, P.; Mayer, P. Carbohydrate-metal complexes: Structural Chemistry of Stable Solution Species. In *Glycoscience*; Springer: Berlin/Heidelberg, Germany, 2008; pp. 1077–1139. [CrossRef]
11. Sharma, P.; Kumar, V.; Guleria, P. Naringin: Biosynthesis and pharmaceutical applications. *Indian J. Pharm. Sci.* **2019**, *89*, 988–999. [CrossRef]
12. Kumar, S.; Pandey, A.K. Chemistry and biological activities of flavonoids: An overview. *Sci. World J.* **2013**, *2013*, 162750. [CrossRef]
13. Sharma, M.; Dwivedi, P.; Singh Rawat, A.K.; Dwivedi, A.K. Nutrition nutraceuticals: A proactive approach for healthcare. In *Nutraceuticals*; Elsevier Inc.: Amsterdam, The Netherlands, 2016; pp. 79–116. [CrossRef]
14. Chen, R.; Qi, Q.L.; Wang, M.T.; Li, Q.Y. Therapeutic potential of naringin: An overview. *Pharm. Biol.* **2016**, *54*, 3203–3210. [CrossRef]
15. Zhao, Y.; Liu, S. Bioactivity of naringin and related mechanisms. *Pharmazie* **2021**, *76*, 359–363. [CrossRef] [PubMed]
16. Zaragoz, C.; Villaescusa, L.; Monserrat, J.; Zaragoz, F.; Melchor, A. Potential therapeutic anti-inflammatory and immunomodulatory effects of dihydroflavones, flavones, and flavonols. *Molecules* **2020**, *25*, 1017. [CrossRef]
17. Qi, Z.; Xu, Y.; Liang, Z.; Li, S.; Wang, J.; Wei, Y.; Dong, B. Naringin ameliorates cognitive deficits via oxidative stress, proinflammatory factors and the PPARγ signaling pathway in a type 2 diabetic rat model. *Mol. Med. Rep.* **2015**, *12*, 7093–7101. [CrossRef]
18. Viswanatha, G.L.; Shylaja, H.; Moolemath, Y. The beneficial role of Naringin- a citrus bioflavonoid, against oxidative stress-induced neurobehavioral disorders and cognitive dysfunction in rodents: A systematic review and meta-analysis. *Biomed. Pharmacother.* **2017**, *94*, 909–929. [CrossRef] [PubMed]
19. Memariani, Z.; Qamar Abbas, S.; Shams ul Hassan, S.; Ahmadi, A.; Chabra, A. Naringin and naringenin as anticancer agents and adjuvants in cancer combination therapy: Efficacy and molecular mechanisms of action, a comprehensive narrative review. *Pharmacol. Res.* **2021**, *171*, 105264. [CrossRef]
20. Amin Hussen, N.H. Docking Study of Naringin Binding with COVID-19 Main Protease Enzyme. *Iraqi J. Pharm. Sci.* **2020**, *29*, 231–238. [CrossRef]
21. Etcheverry, S.B.; Ferrer, E.G.; Naso, L.; Rivadeneira, J.; Salinas, V.; Williams, P.A.M. Antioxidant effects of the VO(IV) hesperidin complex and its role in cancer chemoprevention. *J. Biol. Inorg. Chem.* **2008**, *13*, 435–447. [CrossRef]
22. Naso, L.; Martínez, V.R.; Lezama, L.; Salado, C.; Valcarcel, M.; Ferrer, E.G.; Williams, P.A.M. Antioxidant, anticancer activities and mechanistic studies of the flavone glycoside diosmin and its oxidovanadium(IV) complex. Interactions with bovine serum albumin. *Bioorg. Med. Chem.* **2016**, *24*, 4108–4119. [CrossRef] [PubMed]
23. Goitia, H.; Quispe, P.; Naso, L.G.; Martínez, V.R.; Rey, M.; Rizzi, A.C.; Ferrer, E.G.; Williams, P.A.M. Interactions of rutin with the oxidovanadium(IV) cation. Anticancer improvement effects of glycosylated flavonoids. *New J. Chem.* **2019**, *43*, 17636–17646. [CrossRef]
24. Pessoa, J.C.; Etcheverry, S.; Gambino, D. Vanadium compounds in medicine. *Chem. Rev.* **2015**, *301–302*, 24–48. [CrossRef]
25. Islas, M.S.; Naso, L.G.; Lezama, L.; Valcarcel, M.; Salado, C.; Roura-Ferrer, M.; Ferrer, E.G.; Williams, P.A.M. Insights into the mechanisms underlying the antitumor activity of the new coordination complex with oxidovanadium(IV) and naringenin. Albumin binding studies. *J. Inorg. Biochem.* **2015**, *149*, 12–24. [CrossRef]
26. Chasteen, N.D. *Biological Magnetic Resonance*; Berliner, L.J., Reuben, J., Eds.; Plenum: New York, NY, USA, 1981; p. 3.
27. Gorelsky, S.; Micera, G.; Garribba, E. The Equilibrium Between the Octahedral and Square Pyramidal Form and the Influence of an Axial Ligand on the Molecular Properties of $V^{IV}O$ Complexes: A Spectroscopic and DFT Study. *Chem. Eur. J.* **2010**, *16*, 8167–8180. [CrossRef] [PubMed]

28. Sanna, D.; Ugone, V.; Lubinu, G.; Micera, G.; Garribba, E. Behavior of the potential antitumor VIVO complexes formed by flavonoid ligands. 1. Coordination modes and geometry in solution and at the physiological pH. *J. Inorg. Biochem.* **2014**, *140*, 173–184. [CrossRef] [PubMed]

29. Kivelson, D.; Lee, S. ESR Studies and the Electronic Structure of Vanadyl Ion Complexes. *J. Chem. Phys.* **1964**, *41*, 1896–1903. [CrossRef]

30. Chand, P.; Murali Krishna, R.; Lakshamana Rao, J.; Lakshaman, S.V.J. EPR and optical studies of vanadyl complexes in two host-crystals of tutton salts of thallium. *Rad. Eff. Def. Solids* **1993**, *127*, 245–254. [CrossRef]

31. Liu, K.T.; Yu, J.T.; Lou, S.H.; Lee, C.H.; Huang, Y.; Lii, K.H.J. Electron paramagnetic resonance study of V^{4+}-doped $KTiOPO_4$ single crystals. *Phys. Chem. Solids* **1994**, *55*, 1221–1226.

32. Ferrer, E.G.; Salinas, M.V.; Correa, M.J.; Naso, L.; Barrio, D.A.; Etcheverry, S.B.; Lezama, L.; Rojo, T.; Williams, P.A.M. Synthesis, characterization, antitumoral and osteogenic activities of quercetin vanadyl(IV) complexes. *J. Biol. Inorg. Chem.* **2006**, *11*, 791–801. [CrossRef]

33. Pereira, R.M.S.; Andrades, N.E.D.; Paulino, N.; Sawaya, A.C.H.F.; Eberlin, M.N.; Marcucci, M.C.; Marino Favero, G.; Novak, E.M.; Bydlowski, S.P. Synthesis and Characterization of a Metal Complex Containing Naringin and Cu, and its Antioxidant, Antimicrobial, Antiinflammatory and Tumor Cell Cytotoxicity. *Molecules* **2007**, *12*, 1352–1366. [CrossRef]

34. Naso, L.G.; Lezama, L.; Valcarcel, M.; Salado, C.; Villacé, P.; Kortazar, D.; Ferrer, E.G.; Williams, P.A.M. Bovine serum albumin binding, antioxidant and anticancer properties of an oxidovanadium(IV) complex with luteolin. *J. Inorg. Biochem.* **2016**, *157*, 80–93. [CrossRef] [PubMed]

35. Fanali, G.; di Masi, A.; Trezza, V.; Marino, M.; Fasano, M.; Ascenzi, P. Human serum albumin: From bench to bedside. *Mol. Asp. Med.* **2012**, *33*, 209–290. [CrossRef]

36. Weinryb, I.; Steiner, R.F. The Luminescence of the Aromatic Amino Acids. In *Excited States of Proteins and Nucleic Acids*; Steiner, R.F., Weinryb, I., Eds.; Springer: Boston, MA, USA, 1971. [CrossRef]

37. Lakowicz, J.R. *Principles of Fluorescence Spectroscopy*; Springer Science & Business Media: New York, NY, USA, 2013.

38. Sun, Y.; Zhang, H.; Sun, Y.; Zhang, Y.; Liu, H.; Cheng, J.; Bi, S.; Zhang, H. Study of interaction between protein and main active components in *Citrus aurantium* L. by optical spectroscopy. *J. Luminescence* **2010**, *130*, 270–279. [CrossRef]

39. Kragh-Hansen, U.; Chuang, V.T.G.; Otagiri, M. Practical aspects of the ligand-binding and enzymatic properties of human serum albumin. *Biol. Pharm. Bull.* **2002**, *25*, 695–704. [CrossRef]

40. Zhang, X.; Li, L.; Xu, Z.; Liang, Z.; Su, J. Investigation of the Interaction of Naringin Palmitate with Bovine Serum Albumin: Spectroscopic Analysis and Molecular Docking. *PLoS ONE.* **2013**, *8*, e59106. [CrossRef]

41. Roy, A.S.; Tripathy, D.R.; Chatterjee, A.; Dasgupta, S. A spectroscopic study of the interaction of the antioxidant naringin with bovine serum albumin. *J. Biophys. Chem.* **2010**, *1*, 141–152. [CrossRef]

42. Shi, J.; Cao, H. Molecular structure-affinity relationship of dietary flavonoids for bovine serum albumin. *Braz. J. Pharmacogn.* **2011**, *21*, 594–600. [CrossRef]

43. Karami, K.; Mehri Lighvan, Z.; Farrokhpour, H.; Dehdashti Jahromi, M.; Momtazi-borojeni, A.A. Synthesis and spectroscopic characterization study of new palladium complexes containing bioactive O,O-chelated ligands: Evaluation of the DNA/protein BSA interaction, in vitro antitumoural activity and molecular docking. *J. Biomol. Struct. Dyn.* **2018**, *36*, 3324–3340. [CrossRef] [PubMed]

44. Badea, M.; Olar, R.; Uivarosi, V.; Marinescu, V.; Aldea, V. Synthesis and characterization of some vanadyl complexes with flavonoid derivatives as potential insulin-mimetic agents. *J. Therm. Anal. Calorim.* **2012**, *107*, 279–285. [CrossRef]

45. Perillo, B.; Di Donato, M.; Pezone, A.; Di Zazzo, E.; Giovannelli, P.; Galasso, G.; Castoria, G.; Migliaccio, A. ROS in cancer therapy: The bright side of the moon. *Exp. Mol. Med.* **2020**, *52*, 192–203. [CrossRef]

46. Yoshinaga, A.; Kajiya, N.; Oishi, K.; Kamada, Y.; Ikeda, A.; Chigwechokha, P.K.; Kibe, T.; Kishida, M.; Kishida, S.; Komatsu, M.; et al. NEU3 inhibitory effect of naringin suppresses cancer cell growth by attenuation of EGFR signaling through GM3 ganglioside accumulation. *Eur. J. Pharmacol.* **2016**, *782*, 21–29. [CrossRef] [PubMed]

47. Nie, Y.; Wu, H.; Li, P.; Xie, L.; Luo, Y.; Shen, J.; Su, W. Naringin attenuates EGF-induced MUC5AC secretion in A549 cells by suppressing the cooperative activities of MAPKs-AP-1 and IKKs-IkB-NF-kB signaling pathways. *Eur. J. Pharmacol.* **2012**, *690*, 207–213. [CrossRef]

48. Atta, E.M.; Hegab, K.H.; Abdelgawad, A.A.M.; Youssef, A.A. Synthesis, characterization and cytotoxic activity of naturally isolated naringin-metal complexes. *Saudi Pharm. J.* **2019**, *27*, 584–592. [CrossRef] [PubMed]

49. Qian, J.; Li, J.; Ding, J.; Wang, Z.; Zhang, W.; Hu, G. Erlotinib activates mitochondrial death pathways related to the production of reactive oxygen species in the human non-small cell lung cancer cell line A549. *Clin. Exp. Pharm. Physiol.* **2009**, *36*, 487–494. [CrossRef]

50. Chidambara Murthy, K.; Kim, J.; Vikram, A.; Patil, B.S. Differential inhibition of human colon cancer cells by structurally similar flavonoids of citrus. *Food Chem.* **2012**, *132*, 27–34. [CrossRef] [PubMed]

51. Onishi, H. *Photometric Determination of Traces of Metals*, 4th ed.; John Wiley and Sons, Inc.: New York, NY, USA, 1986.

52. Ali, I.; Wani, W.A.; Saleem, K. Empirical formulae to molecular structures of metal complexes by molar conductance. *Synth. React. Inorg. Met. Nano-Metal Chem.* **2013**, *43*, 1162–1170. [CrossRef]

53. Martínez Medina, J.J.; Naso, L.G.; Pérez, A.L.; Rizzi, A.; Okulik, N.B.; Ferrer, E.G.; Williams, P.A.M. Apigenin oxidovanadium(IV) cation interactions. Synthesis, spectral, bovine serum albumin binding, antioxidant and anticancer studies. *J. Photochem. Photobiol. A Chem.* **2017**, *344*, 84–100. [CrossRef]

54. Hissin, P.J.; Hilf, R. A fluorometric method for determination of oxidized and reduced glutathione in tissues. *Anal. Biochem.* **1976**, *74*, 214–226. [CrossRef]

55. Bradford, M.M. A rapid and sensitive method for the quantitation of microgram quantities of protein utilizing the principle of protein-dye binding. *Anal. Biochem.* **1976**, *72*, 248–254. [CrossRef]

56. Zamzami, N.; Métivier, D.; Kroemer, G. Quantitation of mitochondrial transmembrane potential in cells and in isolated mitochondria. *Methods Enzymol.* **2000**, *322*, 208–213. [CrossRef]